ELSEVIER

Contents lists available at ScienceDirect

# Journal of Magnetism and Magnetic Materials

journal homepage: www.elsevier.com/locate/jmmm





# Phase and d-d hybridization control via electron count for material property control in the X<sub>2</sub>FeAl material class

Ka Ming Law, Ridwan Nahar, Riley Nold, Michael Zengel, Justin Lewis, Adam J. Hauser

Department of Physics and Astronomy, The University of Alabama, Tuscaloosa, AL 35487

#### ARTICLE INFO

Keywords:
DFT
Heusler
Intermetallic
Alloy
Anti-site disorder
DOS
Slater-Pauling
Band structure
Phase stability

#### ABSTRACT

First-principles calculations are performed for full (L2<sub>1</sub>) and inverse (XA) Heusler compounds  $X_2$ FeAl, where X comprise a range of 3d (Sc, Ti, V, Cr), 4d (Y, Zr, Nb, Mo), and 5d (Hf, Ta, W) early and middle column transition metal elements. The formation energy difference between full and inverse phase and the degree of d-d orbital hybridization with increasing total valence electron count are shown to drive the magnetic properties (total and atomic magnetic moments, spin polarization) and electronic properties (band structure and projected density of states) of the material system. Specifically, X-site atomic magnetic moments take on increasingly Fe character with increasing valence electron count, in both full and inverse Heusler phases. This can be explained by changes on the degree of d-d hybridization between X- and Fe-site d orbitals. Synchronized energy shifts in the PDOS of the X- and Y-sites (Fe) across each of the full and inverse Heusler series provide us insight to controlling spin polarization via composition. This work demonstrates the need to holistically study the thermodynamic phase stability, magnetic moments, and spin polarization of Heusler alloys, in the framework of anti-site disorder and in a wider compositional context. The end goal of this study is to benefit the mapping of experimental results in search of a specific property, by providing a methodology for extrapolating properties based on experimental or theoretical results.

# 1. Introduction

Half metallicity refers to a type of band configuration wherein the Fermi level is populated by electronic states belonging to only one spin channel; when a regular charge current is pushed through the material acting as e.g. a spin injector in the context of spin valves[1,2], or a pinned layer in the context of magnetic tunneling junctions[3–5], scattering processes lead to high "spin-polarization" in the outgoing current. Thus, half-metallic materials are ideal candidates for exploring spin-charge transport; when placed into an appropriate heterostructure geometry, they enable spin-charge current switching, which has novel magnetic memory applications.

The search for half-metallic and high spin-polarization compounds has been the major driving force behind *ab initio* (namely, density-functional theory) research in Heusler compounds [6–9] since predictions were made by de Groot et al. [10]. The Heusler material class describes a compound with four interpenetrating FCC lattices, each one occupied by one or no elements. Different Heusler phases differ in the placement of elements on each of the four lattice sites. Heusler

compounds were among the earliest materials in which emergent magnetism and half-metallicity are predicted to be possible (for an overview, see introduction of [11]). A large amount of effort is required to search for half-metallic and high spin-polarization Heusler compounds, since the material class encompasses a giant elemental phase-space—in principle, three of the four lattice sites can be occupied by one of thirty different transition metal elements. Transition metals have the atomic sizes and electron counts that enable stable Heusler ( $X_2YZ$ ) phases when chosen for the X or Y sites, and even limiting to affordable choices for technological scale-up, thousands of possibilities emerge. Among these compounds, many have been predicted to have a high spin polarization (>70 %), which would significant improve device performance over current ferromagnetic materials [12].

It has long been agreed upon within the scientific community that a combination of atomic disorder and/or inhomogeneity in the sample on a nano- or microscopic scale will affect the spin polarization of the material. Unsurprisingly, spin polarization often decreases with increase in atomic disorder. High spin-polarization Heusler compounds would be highly prized in the scientific community when they are stable as a

E-mail address: ahauser@ua.edu (A.J. Hauser).

<sup>\*</sup> Corresponding author.

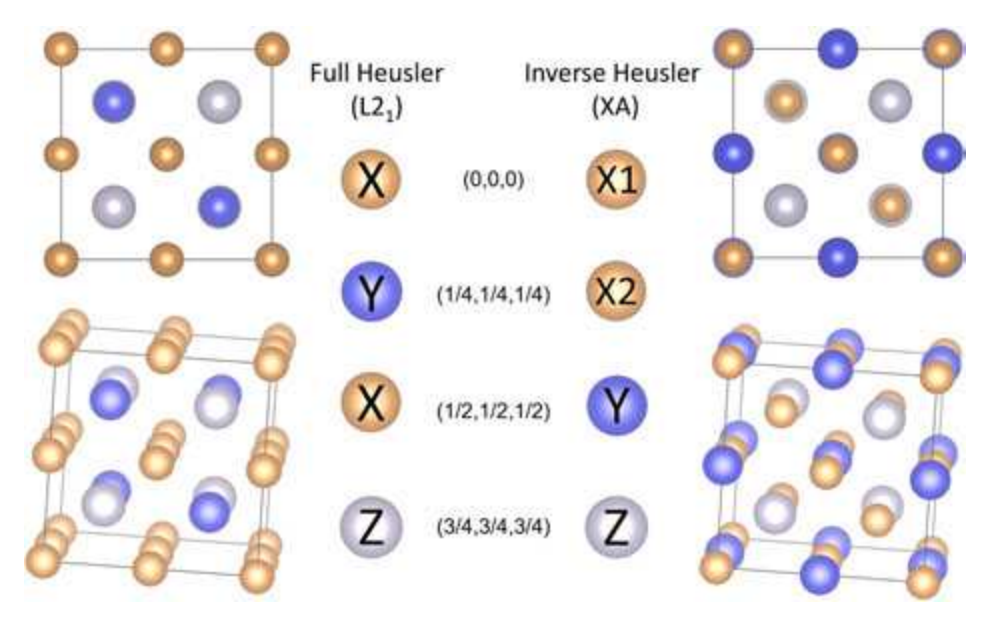


Fig. 1. Atomic structure of full (L2<sub>1</sub>) and inverse (XA) Heusler structures.

Table 1 DFT computation results for full (L2<sub>1</sub>) and inverse (XA) phase  $X_2$ FeAl, where X = 3d, 4d, 5d early transition metal elements.

Compound	Structure	Lattice parameter (Å)	E <sub>FH-IH</sub> (eV/atom)	Magnetic moment $(\mu_B)$					Spin-pol (abs %)
				atom X1	atom X2	atom Y	atom Z	Total (µ <sub>B</sub> /f.u.)	
Sc <sub>2</sub> FeAl	L21	6.538	-0.11706	-0.14	-0.14	1.02	-0.05	0.51	5
Sc <sub>2</sub> FeAl	XA	6.460		-0.22	-0.18	1.52	-0.02	0.91	81
Ti <sub>2</sub> FeAl	L21	6.204	-0.04436	-0.19	-0.19	1.51	0.01	0.99	79
Ti <sub>2</sub> FeAl	XA	6.116		-0.85	-0.58	0.89	-0.02	-1.00	100
V <sub>2</sub> FeAl	L21	5.988	0.15980	0.36	0.36	1.87	0.02	2.72	31
V <sub>2</sub> FeAl	XA	5.935		1.66	-0.20	1.14	0.01	2.92	14
Cr <sub>2</sub> FeAl	L21	5.863	0.15049	1.78	1.78	1.09	0.01	4.97	16
Cr <sub>2</sub> FeAl	XA	5.769		1.35	-1.06	0.67	0.01	1.01	83
Y <sub>2</sub> FeAl	L21	7.063	-0.20208	-0.17	-0.17	2.02	-0.07	1.28	44
Y <sub>2</sub> FeAl	XA	6.884		-0.24	-0.24	1.96	-0.05	1.00	100
Zr <sub>2</sub> FeAl	L21	6.625	-0.21860	-0.17	-0.17	1.70	0.02	1.13	71
Zr <sub>2</sub> FeAl	XA	6.504		0.28	-0.03	0.64	0.00	0.96	65
Nb <sub>2</sub> FeAl	L21	6.345	-0.03861	0.01	0.01	2.10	0.04	2.17	3
Nb <sub>2</sub> FeAl	XA	6.310		0.89	-0.06	1.66	0.01	2.80	2
Mo <sub>2</sub> FeAl	L21	6.136	0.08014	-0.09	-0.09	2.14	0.03	1.92	26
Mo <sub>2</sub> FeAl	XA	6.098		0.22	-0.14	0.91	-0.01	0.98	60
Hf <sub>2</sub> FeAl	L21	6.542	-0.26636	-0.15	-0.15	1.58	0.03	1.07	82
Hf <sub>2</sub> FeAl	XA	6.459		0.14	-0.02	0.50	0.00	0.64	34
Ta <sub>2</sub> FeAl	L21	6.326	-0.08345	0.04	0.04	2.03	0.06	2.20	5
Ta <sub>2</sub> FeAl	XA	6.322		0.77	0.04	1.65	0.01	2.82	50
W <sub>2</sub> FeAl	L21	6.138	0.12006	-0.06	-0.06	2.04	0.04	1.91	28
W <sub>2</sub> FeAl	XA	6.127		0.17	-0.10	0.87	-0.01	0.92	73

single phase, as well as either (1) thermodynamically resilient to atomic disorder or (2) has properties that are robust against inevitable atomic disorder. For instance,  $Co_2FeSi$  has been shown to have a stubborn 50–60 % spin polarization range (point-contact Andreev reflection/PCAR measurements)[13–15] regardless of growth techniques or conditions.  $Co_2MnSi$  is shown to have a spin polarization of a similar range using point-contact Andreev reflection[16] and nonlocal spin valve[17] measurements (in the latter study, assumption on spin diffusion length of  $Co_2MnSi$  was made), or even found to be significantly lower using spin-resolved photoemission spectroscopy[18]. Each of the above studies have suggested that their respective material falls into the second case i.e. in which significantly lower-than-expected yet robust spin polarization is featured in the presence of prevalent and persistent atomic disorder.

Thus, while the search for breakthrough materials with high property metrics is exciting and enjoyable, practical aspects such as thermodynamic stability are non-negligible. High-throughput strategies

solve this problem by surveying a large set of elemental combinations, then filter for compounds with a desirable value range of certain calculated properties. However, these large-scale studies describe materials with perfect crystallinity. While simplification of interesting material systems by idealization is often a good starting strategy, important questions pertaining to the effects on material properties due to varying degrees of atomic disorder are currently outside the scope of these studies.

There are some studies in which the authors investigate the correlation between atomic disorder and properties of interest e.g. total magnetic moment and spin polarization for a single or couple promising Heusler compounds. They simulated the random distribution of atomic disorder between either Y and Z site (B2 disorder) or full randomization of all sites (A2 disorder), using randomly modified supercell structures. Quantities of interest are calculated for varying concentration and different types of disorder. Such an approach is straightforward and has yielded conclusive results, but is computationally expensive, especially

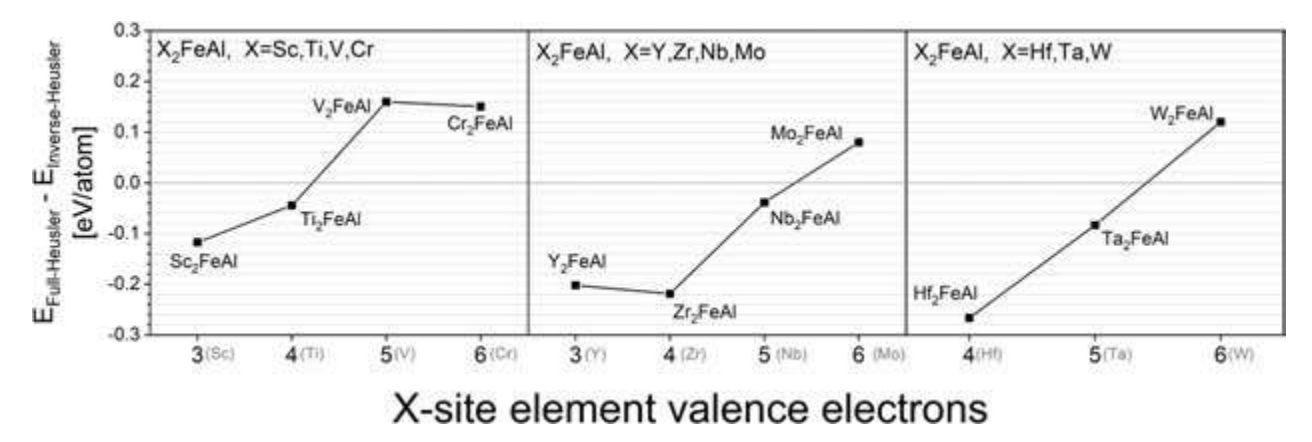


Fig. 2. Difference in formation energies between full and inverse Heusler of the same molecular compound can be seen to fall along a trend with increasing valence electrons on the X-site element.

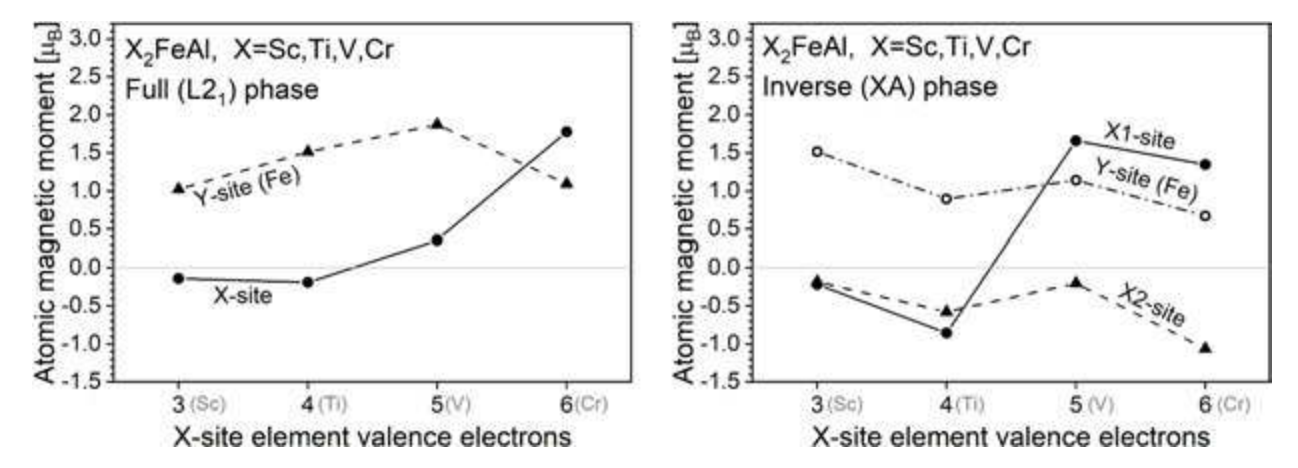


Fig. 3. Calculated atomic magnetic moments of X- and Y- site elements for (a) full and (b) inverse Heusler  $X_2$ FeAl (X = Sc, Ti, V, Cr) as a function of X-site element valence electrons.

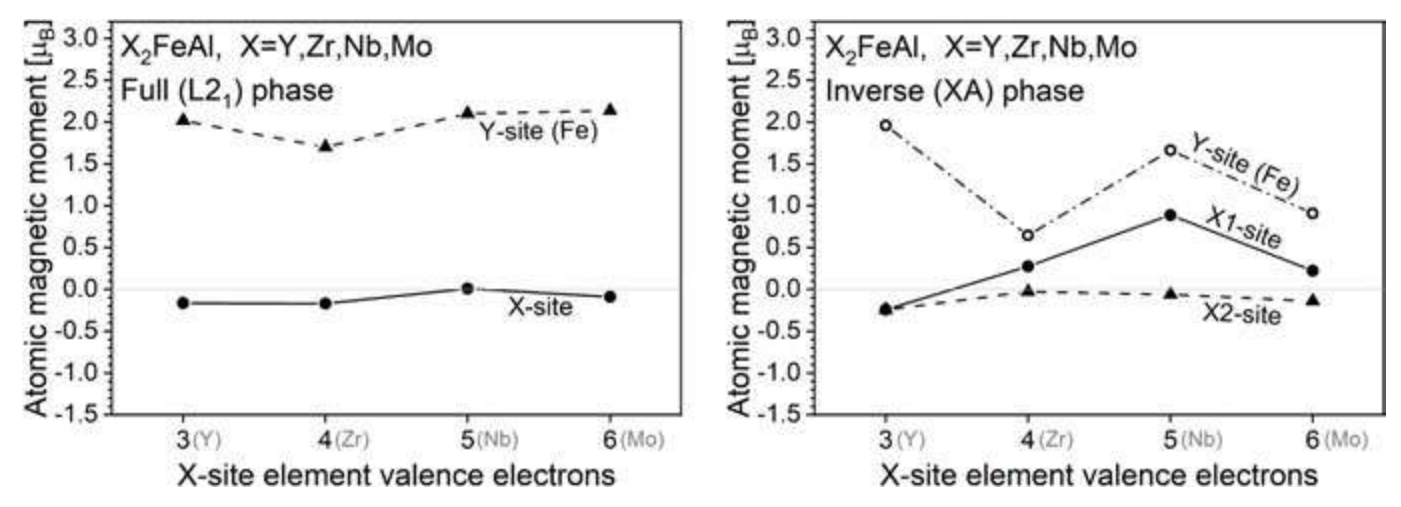


Fig. 4. Calculated atomic magnetic moments of X- and Y- site elements for (a) full and (b) inverse Heusler  $X_2$ FeAl (X = Y,Zr,Nb,Mo) as a function of X-site element valence electrons.

for tertiary Heusler compounds. However, while X and Y sites are typically both transition metals and thus prone to anti-site disorder, studies of the effect of X/Y antisite disorder are less explored due to the difficulty of direct experimental verification.

In this paper, we present a strategy for approximating the magnitude and properties dependencies of atomic disorder on tertiary Heusler

compounds of the form  $X_2YZ$ , where X and Y are transition metals and Z is a post-transition main-group element. Our study is founded on the presumption that a Heusler compound with the stoichiometric formula  $X_2YZ$  will form with no single-element or binary secondary phases, making atomic anti-site disorder the dominant disorder type. As the main-group element Z is more dissimilar to the transition metal X and Y

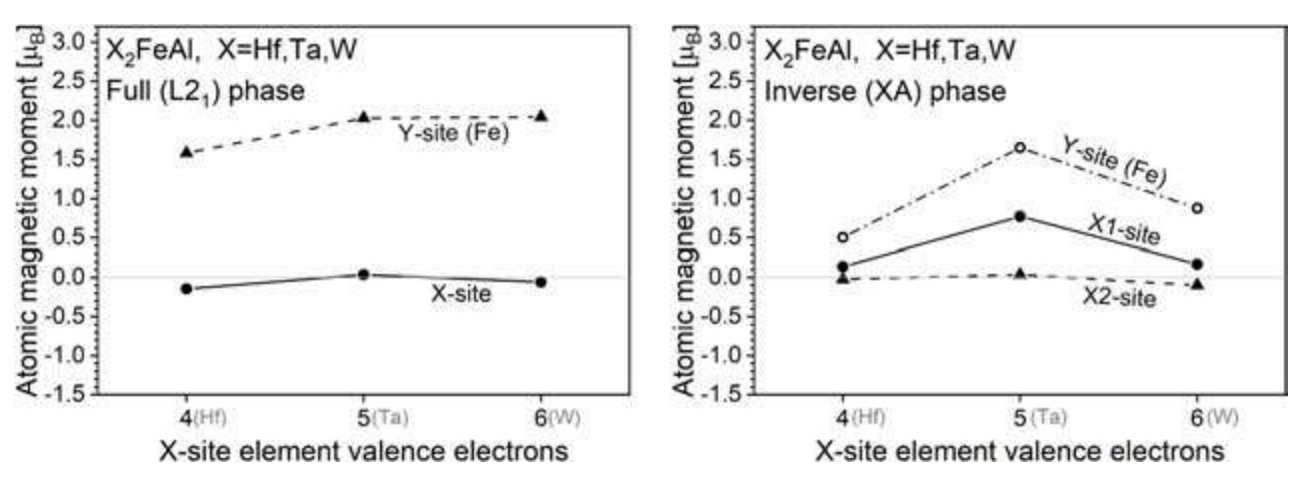


Fig. 5. Calculated atomic magnetic moments of X- and Y- site elements for (a) full and (b) inverse Heusler  $X_2$ FeAl (X = Hf, Ta, W) as a function of X-site element valence electrons.

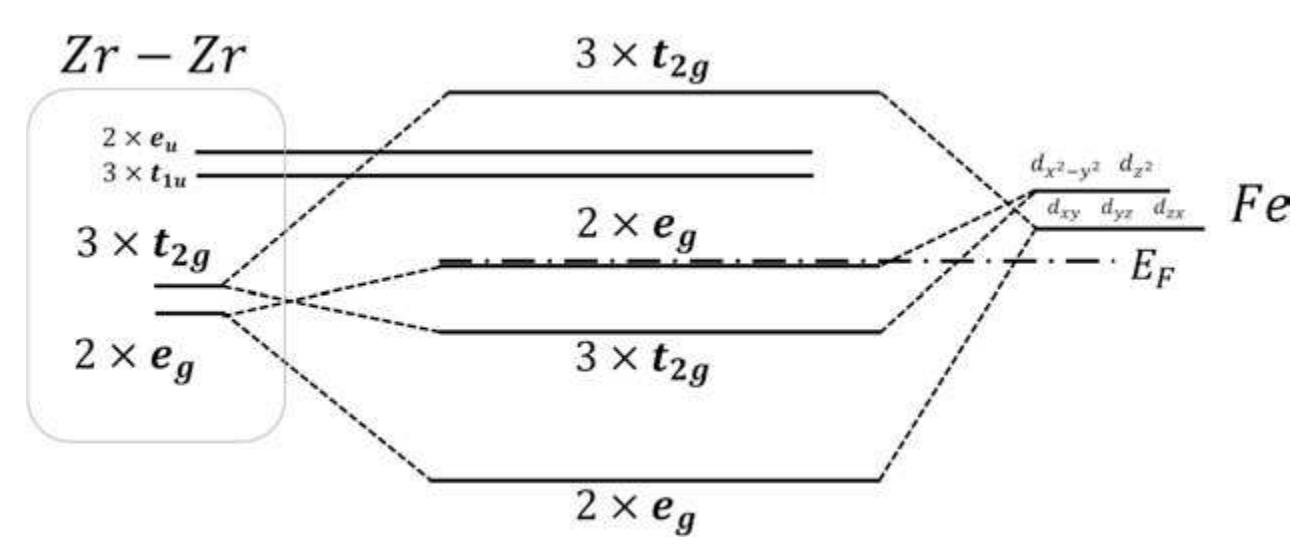


Fig. 6. We propose this model hybridization scheme for  $L2_1$ - $X_2$ FeAl (where X are early transition metals), that agrees with the general Slater-Pauling rule M = N-18. Here, we used X = Zr as an example.

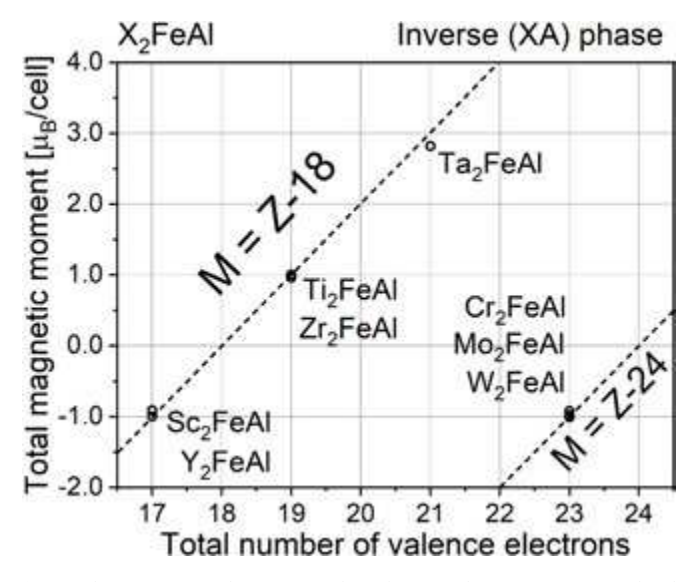


Fig. 7. The inverse Heusler compounds with spin polarization (at Fermi level) in excess of 50% follows the general Slater-Pauling rules.

than they are to each other, we assumed that the X and Y elements swap more readily and focused on this disorder [19,20]. Starting from either the L2 $_1$  (full Heusler) and XA (inverse Heusler) phase, we see that one can arrive at the other phase through increasing concentration of X/Y anti-site disorder (see Fig. 1)—thus, one can consider the scenario where, on a macroscopic scale, the L2 $_1$  and XA phases are two endpoints reached through a series of swaps between X- and Y-site atoms. In this scenario, we posit that the properties of any Heusler alloys with nonnegligible X/Y disorder will sit between those of the purely ordered L2 $_1$  and XA phase. This produces two useful experimental predictions regarding the formation energy difference between the L2 $_1$  and XA phases: it acts as both (1) a metric for the robustness of the lower energy phase against X/Y antisite disorder, and (2) a qualitative measure of how the properties will change with increasing X/Y disorder.

In this paper, we assume that the properties of both full and inverse Heusler phases need to be considered at the *ab-initio* stage, from a practical perspective. In other words, the purpose of our paper is essentially to demonstrate a methodology for evaluating systems without invoking computationally expensive procedures, using Heuslers as an example. There are several previous studies on the L2<sub>1</sub>/XA competition, reporting electronic and magnetic properties of Sc-based [21], Ti-based[22], and V-based[23] Heusler compounds. In contrast to these high-throughput efforts, we investigate a series of compounds and

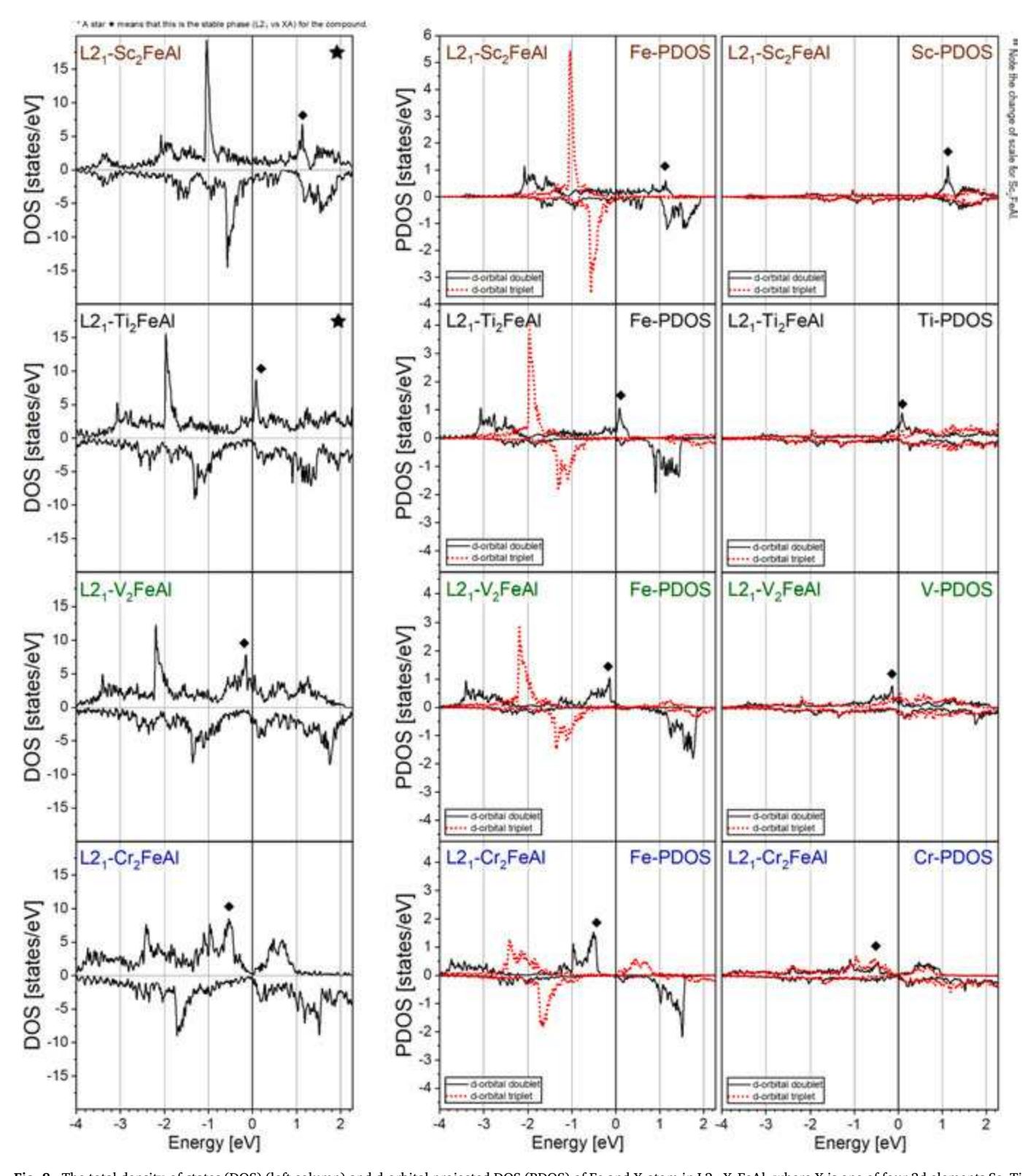


Fig. 8. The total density-of-states (DOS) (left column) and d-orbital projected DOS (PDOS) of Fe and X-atom in L2<sub>1</sub>-X<sub>2</sub>FeAl, where X is one of four 3d elements Sc, Ti, V, and Cr (# of valence electrons = 3,4,5,6). Black and red plots refer to d-orbitals with doublet and triplet degeneracy, respectively. (Please refer to introduction of section IV for more details.) A peak feature (black diamond) is seen to move across the Fermi level in both the total DOS and all respective PDOS. This motion is the main contribution to the change in spin polarization across these compounds. A black star in the DOS graph means that this phase (L2<sub>1</sub>) is the stable phase of the compound. Note the change in scale for  $Sc_2FeAl$  DOS and PDOS. (For interpretation of the references to colour in this figure legend, the reader is referred to the web version of this article.)

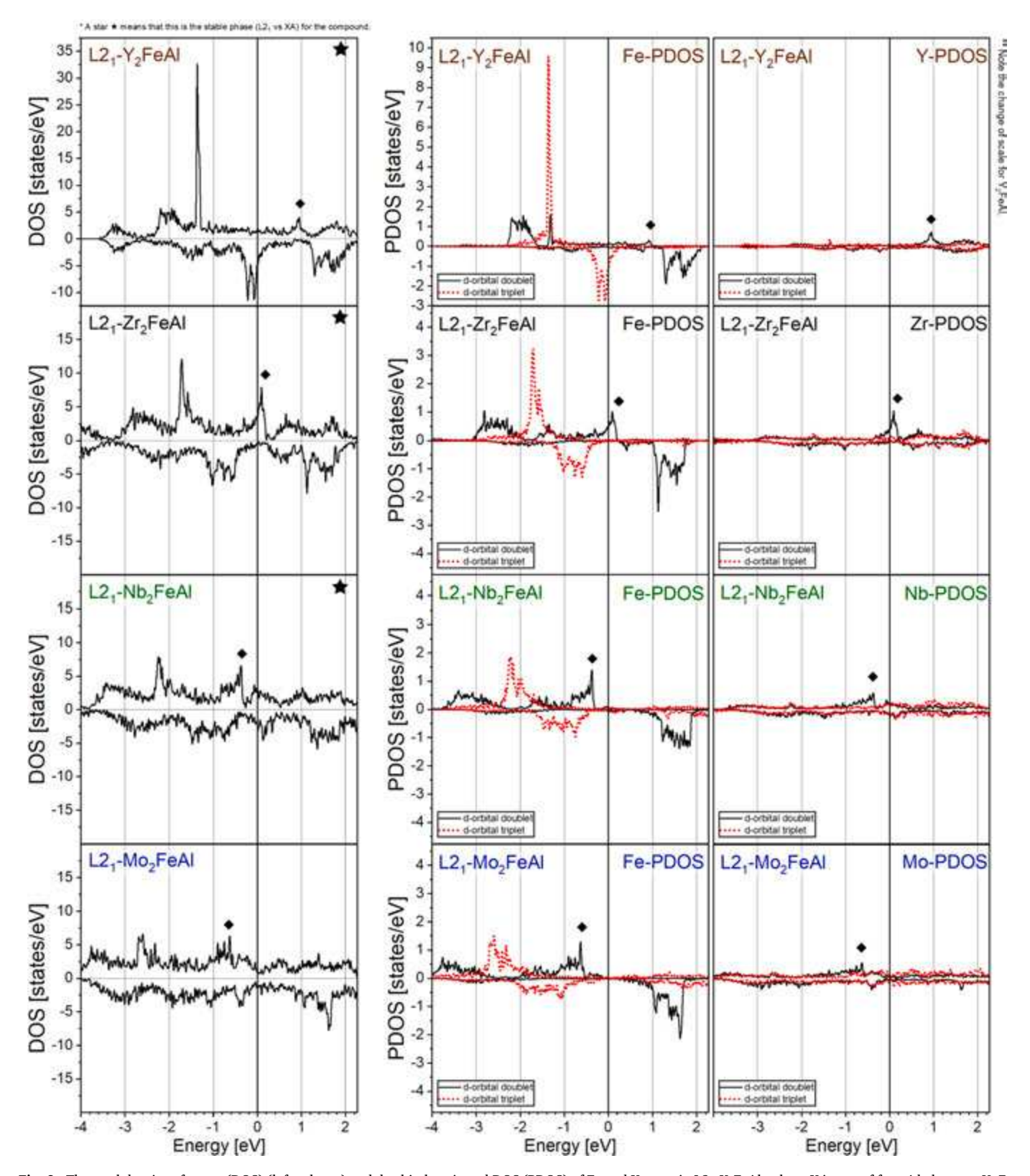


Fig. 9. The total density-of-states (DOS) (left column) and d-orbital projected DOS (PDOS) of Fe and X-atom in  $L2_1$ - $X_2$ FeAl, where X is one of four 4d elements Y, Zr, Nb, and Mo (# of valence electrons = 3,4,5,6). Please see caption of Fig. 8.

dedicate attention to trends among atomic magnetic moments and features within projected density-of-states (PDOS) with varying X-site element. We believe that such discussions at the *ab-initio* stage is informative and acts as a crucial bridge between theoretical and experimental perspectives.

### 2. Methodology

We perform first-principles calculations to examine 11 Heusler compounds containing early to middle transition elements on the X-site. These compounds remained largely unexplored as they most likely have

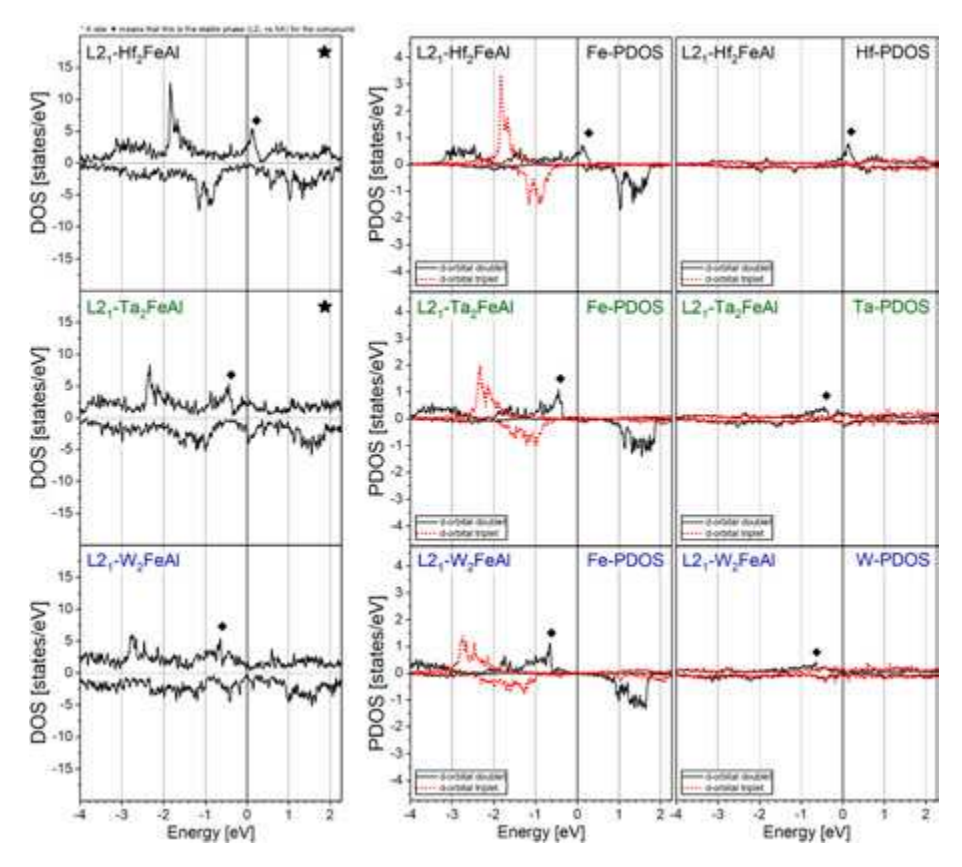


Fig. 10. The total density-of-states (DOS) (left column) and d-orbital projected DOS (PDOS) of Fe and X-atom in L2<sub>1</sub>-X<sub>2</sub>FeAl, where X is one of three 5d elements Hf, Ta, W (# of valence electrons = 4,5,6). Please see caption of Fig. 8.

small total magnetic moment due to their unconventional elemental choices, which we hope can otherwise grant us an insight into the effect of 4d/5d-orbital hybridization. Iron (Fe) is chosen as the Y-site element such that the difference in electronegativity between the X and Y site is at a medium level, and aluminum (Al) is chosen as the Z-site element due its low production cost relative to purity.

#### 2.1. Heusler structure

The Heusler structure is described as four interpenetrating FCC lattices with each FCC lattice arranged equidistant along the {111} direction. Each of the four FCC lattice sites are occupied with a single element. Fig. 1 shows the cubic full (L2<sub>1</sub>) and inverse (XA) Heusler phase crystal structures. Both formulas for full and inverse Heusler compounds are conventionally written as  $X_2YZ$ , but the structures belong to different space groups: the L2<sub>1</sub> phase is  $Fm\overline{3}m$ , and the XA phase is  $F\overline{4}3m$ . In the L2<sub>1</sub> phase, the nearest-neighbor X atoms have octahedral coordination, while the nearest-neighbor Y atoms have tetrahedral coordination; in the XA phase, the single-element coordination is less trivial.

#### 2.2. Computation details

Density functional theory (DFT) calculations are performed using the Quantum Espresso 6.8 package. Our calculations are not DFT + U in this particular study: our compounds do not have large number of valence electrons (relative to e.g.  $Co_2FeSi$ ), thus employing DFT + U for our compounds run the risk of unphysical broadening of the spin-down gap (if present); even the more elaborated GW approach to account for electronic correlations is necessary only in the case of  $Co_2FeSi[24]$ .

Calculations are done using the projector augmented wave (PAW) method in the scheme of generalized gradient approximation (GGA) with scalar-relativistic approximation (SRA); the

Perdew–Burke–Ernzerhof (PBE) pseudopotentials [25] are generated by A. Dal Corso and can be found on the *Quantum Espresso ready-to-use PSlibrary* [26]. We justify our choice for using PBE-parametrized pseudopotentials by pointing out that our calculated density-of-states (DOS) show that our compounds are metallic, despite some being gapped in the spin-down channel; it has been shown that PBE functionals are more appropriate than metaGGA functionals (such as modified Becke-Johnson) for half-metallic ferromagnets [27].

In all calculations, the cutoff energies are not optimized to minimize error in cohesive energies, but instead chosen to be significantly high (wavefunction cutoff energy  $=250~\mathrm{Ry}$ ; charge density cutoff energy  $=1000~\mathrm{Ry}$ ) (Ry = Rydberg; 1 Ry  $=13.6057~\mathrm{eV}$ ). The calculations are spin-polarized, with the atomic starting magnetizations set to either small non-zero values, or large positive or negative values where appropriate—this degree of freedom is utilized to ensure that all possible magnetic ground states of a compound are calculated and considered during the lattice parameter optimization.

The lattice parameter optimization for each compound is done using self-consistent (SCF) calculations; the set of lattice parameter values span across at least 1.000 Å, and the optimal lattice parameter is obtained by fitting the resulting cohesive energy vs unit-cell-volume plot with the Birch-Murnaghan equation of state, by convention of the scientific community. Lattice-relaxation calculations are done using the optimal lattice parameter in the "vc-relax" calculation mode, which utilizes BFGS optimization. Each calculation at this stage is done using the pw.x module, with a 10x10x10 Brillouin zone k-point grid generated using the tetrahedral method, and an energy convergence of  $10^{-7}$  Ry.

A final SCF calculation is performed using a 20x20x20 Brillouin k-point grid and an energy convergence of  $10^{-9}$  Ry instead. Atomic magnetic moments and cohesive energy are extracted from this high-resolution SCF calculation. A single non-self-consistent (NSCF) calculation is performed using the pw.x module in the "nscf" calculation mode

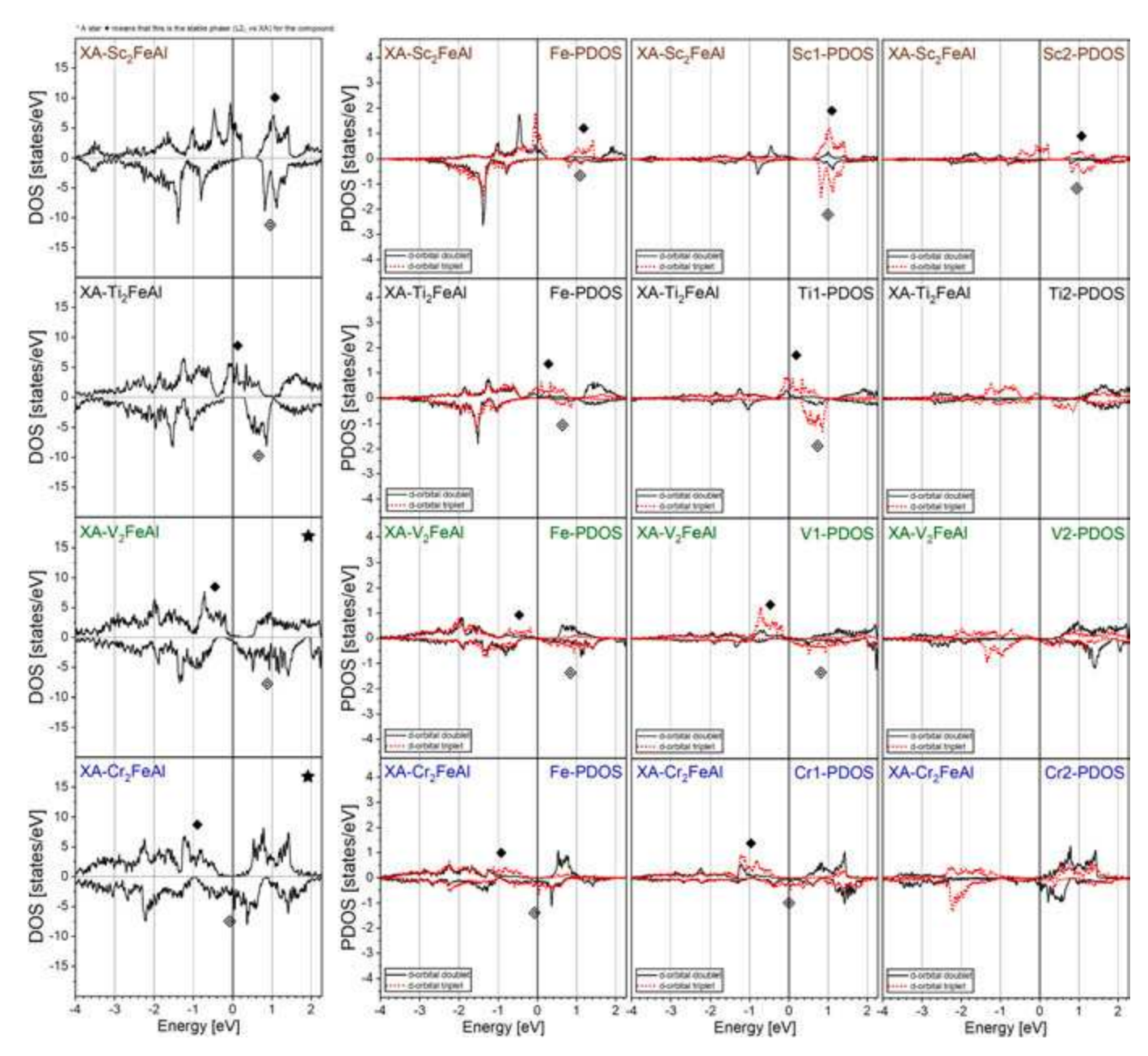


Fig. 11. The total density-of-states (DOS) (left column) and d-orbital projected DOS (PDOS) of Fe and X atom in XA-X<sub>2</sub>FeAl, where X is one of four 3d elements Sc, Ti, V, and Cr (# of valence electrons = 3,4,5,6). Please see caption of Fig. 8.

prior to density-of-states (DOS) and bands calculations. Tests for tetragonality were completed for c/a ratios ranging from 0.95 to 1.05, with the cubic c/a =1 found to be the most energetically favorable ratio across the series. DOS calculations are performed using the dos.x module. The maximum and minimum energies are chosen appropriately on a case-by-case basis (since the position of the Fermi level varies greatly between compounds). The energy resolution is 0.001 eV. Band structure calculations are performed using the pw.x module in the "bands" calculation mode, along k-paths as indicated in the band diagrams of this paper. After the band structure calculation, a band-data reordering process is performed using the bands.x module.

## 3. Results and Discussion

Our computational results in the following are ordered first by group (number of valence electrons)—then by period—of the X-site element. They are summarized in Table 1. Results and discussions are organized

by X-site elemental group where necessary, and molecular formulas will be referred simply as X=(X-site element) where appropriate. We utilize formation energy differences  $\Delta E_{\rm full-inv}$  between full and inverse Heusler phase (full minus inverse) as a quantifier of phase preference in the context of thermodynamics; a negative  $\Delta E_{\rm full-inv}$  value means that the L2 $_1$  phase has a lower formation energy than does the XA phase, regardless of the signs of either formation energy values, thus implying that the L2 $_1$  phase is more thermodynamically stable (at least in comparison to XA). Discussion on specific materials systems of interest can be found in the Supplementary Information section.

The atomic magnetic moment of the Fe site will be set as the positive z-direction unless otherwise specified. This is also the spin-up direction. The rationale for this convention is that a hypothetical external magnetic field in the (001) direction would align the Fe moments along this direction. Spin-polarization values (at the Fermi level) are calculated as follows:

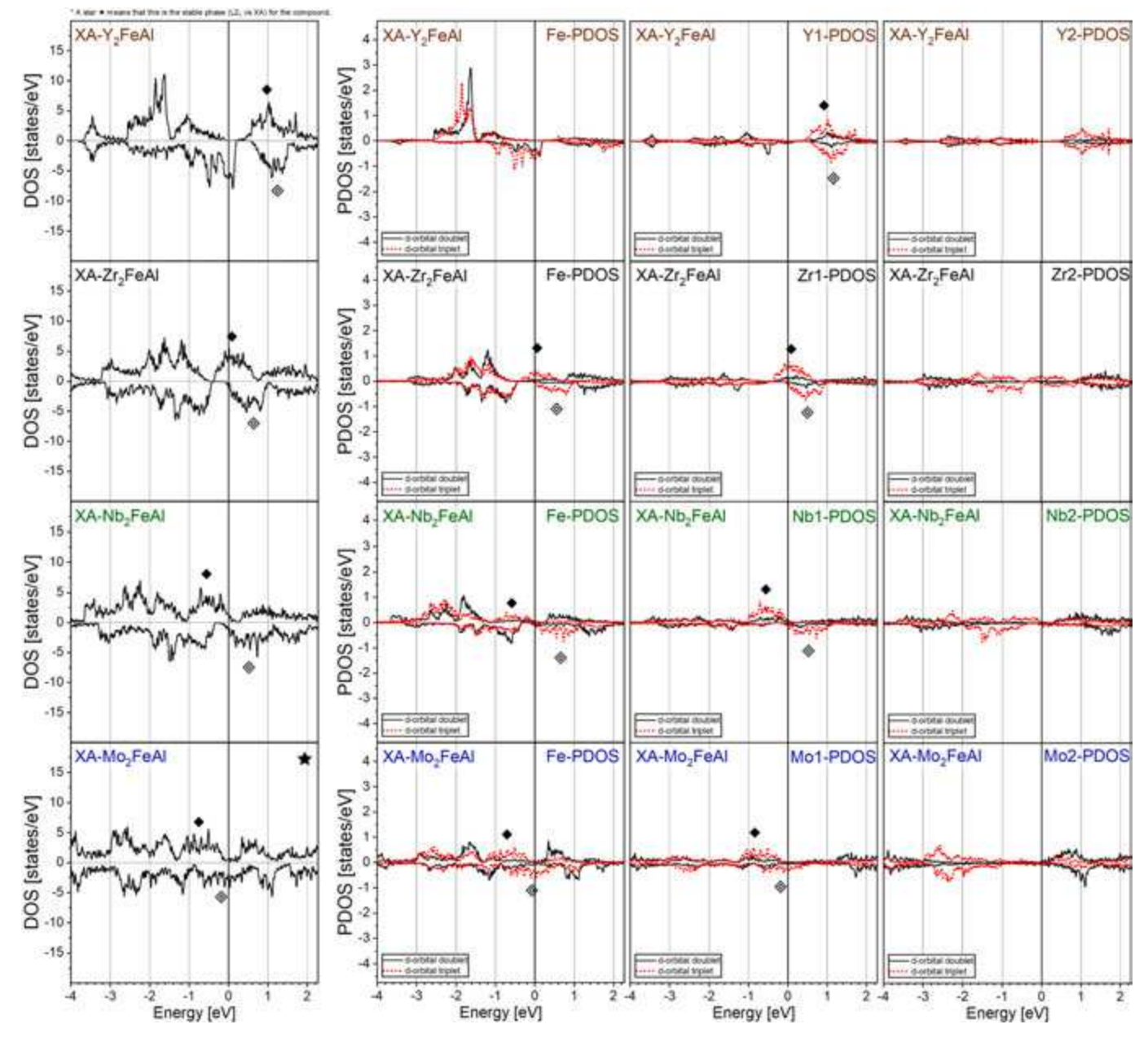


Fig. 12. The total density-of-states (DOS) (left column) and d-orbital projected DOS (PDOS) of Fe and X-atom in XA-X<sub>2</sub>FeAl, where X is one of four 4d elements Y, Zr, Nb, and Mo (# of valence electrons = 3,4,5,6). Please see caption of Fig. 8.

$$P = \frac{N\uparrow - N\downarrow}{N\uparrow + N\downarrow} \times 100\%$$

and will be presented as absolute values.

# 3.1. Formation energy differences and magnetic moments

The difference in formation energy between  $L2_1$  and XA phases provides a measure of the energy scale required to form an unfavored phase over a favored one. In this work, where each swap between X- and Y-site atoms represents a partial step toward one phase and away from the other, we can use this energy as a metric of the likelihood of antisite disorder occurring during formation and/or processing, with larger energy differences suggesting lower likelihood of X/Y site disorder. A general trend in formation energy difference can be seen with increasing atomic number, as one increases the X-site valence electron choice within each orbital subset of X = 3d, 4d, and 5d elements (Fig. 2).

Formation of the XA phase becomes increasingly preferable over the  $L2_1$  phase as the number of valence electrons of the X-site element either 1) increases or 2) approaches that of the Y-site element (Fe). Similar trends among early-transition-metal Heuslers have been observed in previous studies [28–30].

This monotonic trend is slightly broken between (1)  $V_2FeAl$  and  $Cr_2FeAl$  for X=3d elements, and (2)  $Y_2FeAl$  and  $Zr_2FeAl$  for X=4d elements. The deviation from this trend is slight, and it is unclear which of the two compounds in each case represents the actual anomaly. Regardless, the formation energy differences form a clear trend with number of valence electrons on the X-site element.

Atomic magnetic moment data provides some insight into the effects of the L2<sub>1</sub>-XA phase transition as the valence electron count increases, starting with the X = 3d elements in Fig. 3. The X-site moments in L2<sub>1</sub>-Sc<sub>2</sub>FeAl and L2<sub>1</sub>-Ti<sub>2</sub>FeAl (Fig. 3a) are antiparallel to Fe moments, with the Fe moments being the dominant contribution to the total magnetic moment. However, in L2<sub>1</sub>-V<sub>2</sub>FeAl the X-site atomic moments become

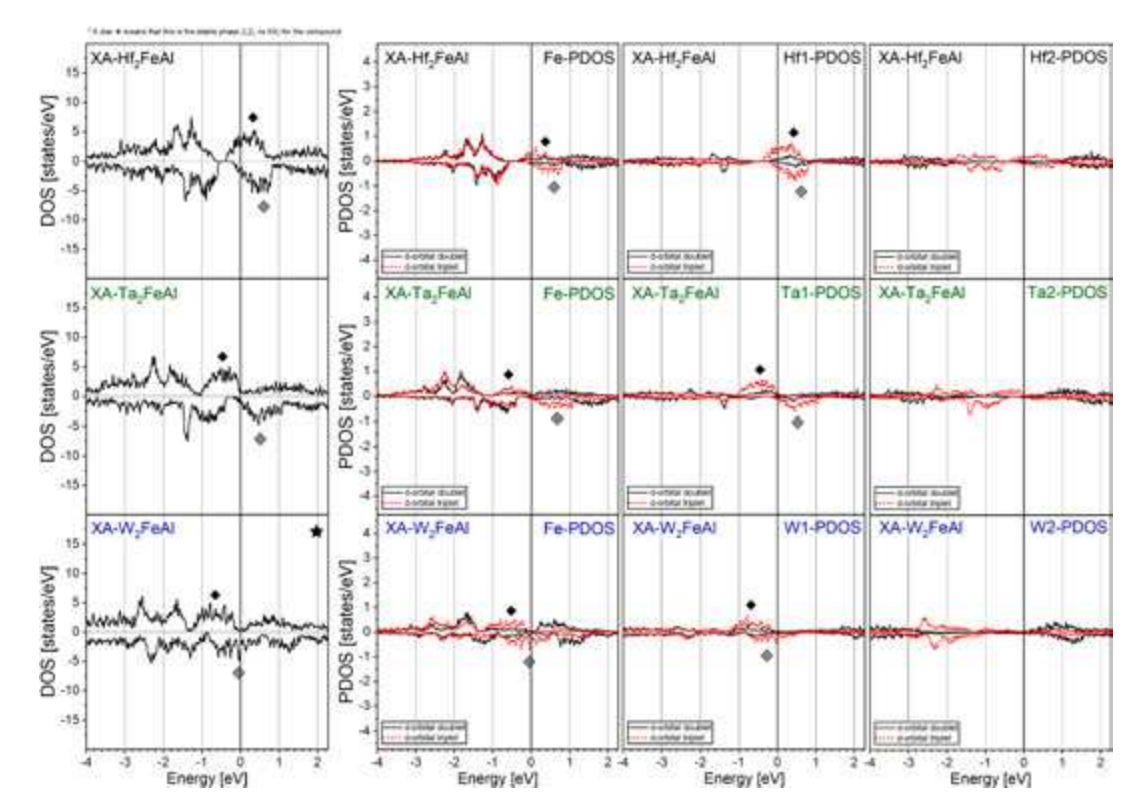


Fig. 13. The total density-of-states (DOS) (left column) and d-orbital projected DOS (PDOS) of Fe and X-atom in XA-X<sub>2</sub>FeAl, where X is one of three 5d elements Hf, Ta, W (# of valence electrons = 4,5,6). Please see caption of Fig. 8.

parallel to the Fe moments and subsequently surpass Fe moments in magnitude in L2<sub>1</sub>-Cr<sub>2</sub>FeAl. Similarly, as we increase valence electrons from XA-Ti<sub>2</sub>FeAl to XA-V<sub>2</sub>FeAl in Fig. 3b, the X1-site atomic moments flip into the direction of the Fe moments. For L2<sub>1</sub> phases, the X-site moments are larger in magnitude than Fe moments when X = Cr, and for XA phases the X1 moment magnitudes exceed that of Fe in X = V.

To understand this, recall that the strength of d-orbital hybridization between X and Y (Fe) atoms generally scales with the similarity between the two electronic orbital wavefunctions [7]. Since outer-shell d-orbitals constitute a large contribution of the magnetic moment of a transitionmetal atom, Fig. 3a demonstrates that as X-site elements are chosen with d-orbital configurations more similar to Fe, increasing d-d hybridization gives the X-site increasingly Fe-like magnetic character. From this result, we posit that the greater hybridization between X and Y atoms in XA phase compared to L2<sub>1</sub> phase is a consequence of the conversion of X atoms (the X1 site) from tetrahedral to octahedral coordination with Y atoms when antisite disorder moves an X-site atom to an erstwhile Y site. The d-d hybridization in this system is stronger when octahedrally coordinated, since the spatial arrangement of the lobes of d-orbitals facilitates better wavefunction overlap with Fe atoms. The stronger average d-d hybridization between X and Fe orbitals explains why the moment reversal at the X1-sites in XA phases begins at X = V in Fig. 3b, instead of X = Cr as does in L2<sub>1</sub> phases. The reversals of X1-site magnetic moments can thus be thought of as the result of a difference in atomic-lattice symmetry.

In the case of X=4d and 5d elements with Y=Fe (which is a 3d transition metal), we expect weaker d-d hybridization between X and Fe atoms compared to the X=3d system regardless of which phase is evaluated. This behavior is observed. The X1-site gains only a smaller magnetic moment in XA phase compared to the X=3d series, as expected. The finer details of the underlying physics appear to hold as we investigate the  $L2_1$  and XA series for the X=4d series as well. We find only small negative or negligible X-site magnetic moments across all calculated  $L2_1$  phases (Fig. 4a), while Fe moments remain

approximately 2  $\mu_B/Fe$  throughout the series, seemingly absent of any hybridization. However, the X1-site magnetic moments show a marked change with valence electron count in the XA phases (Fig. 4b), changing direction from slightly negative (antiparallel to Fe) in  $Y_2FeAl$  to positive (parallel to Fe) in  $Zr_2FeAl$  to  $Mo_2FeAl$ . We note that, in the X=4d element series, the energetically favorable  $L2_1$  phase for  $X=Y,\,Zr,\,Nb$  gives way to XA phase for X=Mo, and a break from the linear change in X1-site moment at X=Mo correlates with the transition from  $L2_1$ -favored compounds to XA-favored  $Mo_2FeAl$  in Fig. 2.

In the X=5d series (Fig. 5), the same pattern holds, with small/negative magnetic moments on the X site for the energetically favorable  $L2_1$  phases for X=Hf, Ta and a positive (albeit not large) X1-site moment for the favored XA phase for X=W. In Fig. 5b, we see that the X1-site moments are further muted compared to the same electron counts for 3d and 4d elements, although we note that it is only a slight falloff. Taken in sum, we tentatively conclude that the orbital number of the electron plays a tangible role in hybridization but is (of course) secondary to the phase formation that creates it in the first place.

#### 3.2. Slater-Pauling behavior

Half-metallic Heusler compounds have been shown to display Slater-Pauling behavior[31–33], wherein their total magnetic moments M are expected to match generalized Slater-Pauling rules of the form M=N-Z, where Z is an integer, and N is the total number of valence electrons of the molecular formula; for half-metallic full Heuslers, the typical Slater-Pauling rule is M=N-24 [6,8,9]; for inverse Heusler compounds, both M=N-18 and M=N-24 rules for magnetization have been proposed in response to observed trends[34]. Generalized Slater-Pauling rules apply best to compounds that have a gapped minority band, as the numerical coefficient in those rules originate from the number of d-orbital energy-levels from specific molecular hybridization schemes. As such, we examine here the 3 full (L2<sub>1</sub>) and 8 inverse (XA) Heusler phases calculated to have spin polarizations greater than 50 % for potential Slater-

Pauling behavior. Before evaluating total magnetic moment as a function of total valence electrons, we readjust the signs of the total magnetic moment for each compound, such that the majority bands (non-gapped) are in the spin-up (+z) direction. This convention is only necessary for, and will only be used for, discussions on Slater-Pauling plots.

Only three L2 $_1$  phases (Ti $_2$ FeAl, Zr $_2$ FeAl, and Hf $_2$ FeAl) in this work have spin polarization larger than 50 %, but we note that they are all energetically favored over their XA phase counterpart. All three have the same total number of valence electrons per compound of 19, and total magnetic moments closely approximating 1  $\mu_B$ /cell thus fitting the N-18 rule instead of the N-24 rule. This result is unconventional at first glance, but both computational and experiment studies of Heuslers with X sites occupied by early transition metals are rare, and the consensus for the more "common" N-24 rule is based primarily on high-moment alloys that have been the focus of studies in the past[6,8,9,34,35].

We propose the d-orbital hybridization scheme in Fig. 6 that would explain the M=N-18 trend for these  $L2_1$  compounds: 18 is 2 times the sum (across all four atomic sites) of all relevant orbitals (energy-levels) with energies under the Fermi level, which includes four s-orbitals (not shown), two  $e_g$  and three  $t_{2g}$  hybridized d-orbitals. In the case of L2<sub>1</sub>-Ti<sub>2</sub>FeAl, Zr<sub>2</sub>FeAl, and Hf<sub>2</sub>FeAl, 18 of the 19 total valence electrons fill all 18 energy levels; the single remaining electron resides in the next higher energy level, which became the Fermi level; since there is only one electron per molecular formula i.e. per unit cell at the Fermi level, the system is half-metallic. We placed the Fermi level at the doublydegenerate  $[X_2Fe]^{3-}$   $\mathbf{e}_{\mathbf{g}}$  energy level, and the  $\mathbf{e}_{\mathbf{u}}$  and  $\mathbf{t}_{1\mathbf{u}}$  energy levels above the Fermi level. This is based on our observation on the projected density-of-states (PDOS) of the X and Fe atomic species; we found that the Fermi level is populated by d-electronic states with a doublydegenerate nature in only one spin channel (Fig. 9), in accordance to our proposed molecular orbital model in Fig. 6.

A plot of the total magnetic moment as a function of valence electrons is shown in Fig. 7 for the 8 out of 11 inverse (XA) Heusler systems calculated to have spin polarization larger than 50 %. Dashed lines show the position of the M = N-24 and M = N-18 Slate-Pauling dependencies common in XA systems. We find that the total magnetic moments of X = Sc,Ti,Y,Zr,Ta follow the M = N-18 rule very closely, while X = Cr,Mo,W lie on a single point of total valence electron = 23 and magnetic moment = -1  $u_B$ , belonging to M = Z-24 (see Fig. 7). Molecular orbit hybridization models have been proposed for these two magnetization rules in [341].

#### 3.3. Spin polarization/PDOS

Projected DOS (PDOS) of X- and Fe- atomic site can provide insight into the origin of high spin-polarization (over 50 %) observed in the L2 $_1$  and XA compounds mentioned in the previous section. Unsurprisingly, we find that the DOS near the Fermi level ( $\pm 7~{\rm eV}$ ) is dominated by dorbitals; thus, our discussions will be solely focused on d-orbital PDOS. The seemingly unconnected spin-polarization values across each period (X = 3d/4d/5d elements) can be explained by coincident shifts in the relative position between the Fermi level and features in the PDOS of the X- and Y-site (Fe) d-orbitals as the X-site choice is modified. In other words, the origin of spin polarization (e.g. the shape of features in a PDOS that constitutes the minority band gap) in this material class is not controlled by a single monolithic feature, even as we simplify the process greatly by holding the Y- and Z-site choices constant. Band diagrams for all calculated compounds are presented at the end in the Supplementary Information, Figures S1-S3.

Within this section, two d-orbitals,  $d_{z2}$  and  $d_{x2-y2}$  have identical PDOS in our computations; these d-orbitals will be referred as the "doublet" orbitals in the following discussions. The other three d-orbitals,  $d_{xy}$ ,  $d_{yz}$ , and  $d_{zx}$  have identical PDOS as well, and will be referred as the "triplet" orbitals.

#### 3.3.1. Full Heuslers (L2<sub>1</sub>)

The total DOS, Fe-PDOS and X-site PDOS for L2<sub>1</sub>-X<sub>2</sub>FeAl where X = 3d, 4d, and 5d elements are shown in Fig. 8, Fig. 9, and Fig. 10 respectively. In each figure, the total DOS are in the first column. A black star ( $\star$ ) on the right top corner of a DOS denotes that the phase (full-Heusler) is the stable phase for the compound, when compared to the inverse Heusler phase. The second and third columns are the Fe-PDOS (common to all material systems) and PDOS of the unique X-site. Note that there is a change of vertical scale for L2<sub>1</sub>-Sc<sub>2</sub>FeAl (Fig. 8) and L2<sub>1</sub>-Y<sub>2</sub>FeAl (Fig. 9).

Across all full-Heusler compounds, the PDOS for the X-site (X-PDOS) (third column) shows an extremely low number of states across all energies, while the (Y-site) Fe-PDOS (second column) features prominent peaks within ± 4 eV of the Fermi level (Fig. 8, Fig. 9, Fig. 10). At nearly every energy, the Fe-PDOS is almost exclusively composed of states from either the doublet (black) or triplet (red) d-orbitals, with only a few having any significant representation from both orbital classes. In the X-PDOS, we observe relatively small state contributions across the series compared to Fe-PDOS, but we note a single doublet orbital contribution peak (marked in figures with black diamond ♠ near the Fermi level that moves in concert with the doublet contribution peak from the Fe site. The coordinated movement in the PDOS of both atomic species suggests that the X-site and Fe d-orbital band(s) are strongly hybridized.

The Fe-PDOS are qualitatively identical across all L21 phases. From low to high energy, one finds a doublet peak, a triplet peak, and a doublet peak, in this order; however, we note that the low-energy doublet peak in the spin-down channel is broad and has comparatively very low densities of states. In the case of X = Ti (Fig. 8), X = Zr(Fig. 9), and X = Hf (Fig. 10) i.e. X valence electrons = 4, the Fermi level sits on the second doublet peak of the Fe-PDOS (this is the aforementioned peak with a matching partner in the X-PDOS); at this energy, there are few to no states in the spin-down channel. This positioning of the Fermi level leads to a high spin-polarization value for these compounds. Interestingly, with an increase in number of valence electrons in the X-element, we find this peak moves through the Fermi level towards lower energy. The spin-polarization values for those compounds are accordingly very small. We are also able to locate this peak in the DOS of  $L2_1$ -Sc<sub>2</sub>FeAl and Y<sub>2</sub>FeAl (Sc and Y has valence electrons = 3), at  $\sim 1$  eV above the Fermi level.

In summary, we observe that the X-site and Fe-site doublet states near the Fermi level move in concert to lower energies with respect to the Fermi energy as electron count is increased. While at first glance, the shift in the relative energy between said peak and the Fermi level can simply be explained by a shift in the Fermi energy due to a change in the total number of valence (d-) electrons in the unit cell, many of the double and triplet states do not maintain their shape, and not all states show the same (or indeed, any) change in energy with electron count. The motion of these doublet states with increasing electron count provides convincing evidence of significant d-d hybridization in Full Heusler phases for X-site choices in the 3d, 4d, and 5d orbital rows alike.

# 3.3.2. Inverse Heuslers (XA)

The total DOS, Fe-PDOS and X-site PDOS for XA-X<sub>2</sub>FeAl where X=3d, 4d, and 5d elements are shown in Fig. 11, Fig. 12, and Fig. 13 respectively. In each figure, the total DOS are in the first column. A black star ( $\star$ ) on the right top corner of a DOS indicates that this phase (inverse-Heusler) is the stable phase for the compound. The second, third, and fourth columns are the Fe-PDOS, X1-PDOS and X2-PDOS. The doublet (black) and triplet (red) states in the Fe-PDOS (second column) of our computed inverse Heusler compounds are not as cleanly separated as those of the full Heusler compounds, with many similar energy positions and feature shapes (Fig. 11, Fig. 12, Fig. 13). As in the full Heuslers, the density-of-states associated to the X (X1 and X2) atomic species (third and fourth column) have generally broad features.

The X1-PDOS also features one peak near the Fermi level that has mostly triplet nature in each spin channel. This channel serves as the primary driver of electronic property differences between full and inverse Heusler phases, and the driver of contribution of high spin polarization in several inverse Heusler compounds. For X elements with 4 valence electrons i.e. X = Ti (Fig. 11), X = Zr (Fig. 12), and X = Hf (Fig. 13), the Fermi level sits at the center of the peak ( $\spadesuit$ ) in the spin-up channel, and on the edge of the peak ( $\diamondsuit$ ) in the spin-down channel—this leads to a high spin-polarization value in those compounds (XA-Ti<sub>2</sub>FeAl, Zr<sub>2</sub>FeAl, and Hf<sub>2</sub>FeAl).

For X elements with 5 valence electrons i.e. X = V (Fig. 11), X = Nb (Fig. 12), and X = Ta (Fig. 13), the peak in the spin-up channel sits below the Fermi level, while the peak in the spin-down channel remain above the Fermi level. Combined with the fact that there is a very small number of electronic states at the Fermi level in the Fe- and X2-PDOS, the resulting spin-polarization of these compounds are nearly negligible. The exception is XA- $Ta_2$ FeAl, in which the difference in number of spin-up/down states is small but significant relative to the total, resulting in a decent spin-polarization value of 50 %.

For X elements with 6 valence electrons i.e. X = Cr (Fig. 11), X = Mo (Fig. 12), and X = W (Fig. 13), the spin-down peak now sits at the Fermi level, and restores high spin-polarization, albeit in the opposite direction. The seemingly independent "motions" of the spin-up peak ( $\spadesuit$ ) and spin-down peak ( $\diamondsuit$ ) lends credit to the idea brought into light earlier—that band energies are being affected by changes to the degree of d-d hybridization that stems from increasing number of total valence electrons per unit cell.

#### 4. Conclusions

We have performed DFT calculations on a L2 $_1$  and XA Heusler compounds X $_2$ FeAl, where X are 3d, 4d, and 5d early transition metal elements. Our calculation results show that X atomic magnetic moments evolve towards the Fe moments with increasing valence electrons on the X element, in both full and inverse Heusler compounds; these trends can in fact be explained by changes on the degree of d-d hybridization imparted by the increasing similitude of X-atom d-orbitals to the Y-atom (Fe) d-orbitals. We pointed out motifs shared between PDOS of the X-and Y-sites (Fe) across each of the full and inverse Heusler phases, and how the synchronized "motions" of these common features relative to the Fermi level provide us a perspective regarding the origin of high spin polarization (or lack thereof).

#### CRediT authorship contribution statement

Ka Ming Law: Conceptualization, Data curation, Investigation, Methodology, Visualization. Ridwan Nahar: Data curation, Investigation, Supervision, Visualization. Riley Nold: Data curation, Investigation. Michael Zengel: Data curation, Investigation. Justin Lewis: Data curation, Investigation. Adam J. Hauser: .

#### Declaration of competing interest

The authors declare that they have no known competing financial interests or personal relationships that could have appeared to influence the work reported in this paper.

#### Data availability

Data will be made available on request.

## Acknowledgements

We acknowledge support from the National Science Foundation (NSF), USA through NSF-CAREER Award No. DMR-2047251.

#### Appendix A. Supplementary data

Supplementary data to this article can be found online at https://doi.org/10.1016/j.jmmm.2024.171932.

#### References

- M. Johnson, R.H. Silsbee, Interfacial charge-spin coupling: injection and detection of spin magnetization in metals, Phys. Rev. Lett. 55 (17) (1985) 1790–1793.
- [2] V. Sharma, et al., Growth temperature-controlled Gilbert damping and anisotropies in PLD grown epitaxial Co2FeSi heusler alloy thin film, AIP Adv. 13 (2) (2023).
- [3] P. Mavropoulos, M. Ležaić, S. Blügel, Half-metallic ferromagnets for magnetic tunnel junctions by ab initiocalculations, Phys. Rev. B 72 (17) (2005).
- [4] W.J. Gallagher, et al., Microstructured magnetic tunnel junctions (invited), J. Appl. Phys. 81 (8) (1997) 3741–3746.
- [5] S. Ikeda, et al., Magnetic tunnel junctions for spintronic memories and beyond, IEEE Trans. Electron Devices 54 (5) (2007) 991–1002.
- [6] I. Galanakis, P.H. Dederichs, N. Papanikolaou, Slater-pauling behavior and origin of the half-metallicity of the full-heusler alloys, Phys. Rev. B 66 (17) (2002).
- [7] I. Galanakis, P.H. Dederichs, N. Papanikolaou, Origin and properties of the gap in the half-ferromagnetic heusler alloys, Phys. Rev. B 66 (13) (2002).
- [8] I. Galanakis, P. Mavropoulos, P.H. Dederichs, Electronic structure and slater-pauling behaviour in half-metallic heusler alloys calculated from first principles, J. Phys. D Appl. Phys. 39 (5) (2006) 765–775.
- [9] G.H. Fecher, et al., Slater-pauling rule and curie temperature of Co2-based heusler compounds, J. Appl. Phys. 99 (8) (2006).
- [10] R.A. de Groot, et al., New class of materials: half-metallic ferromagnets, Phys. Rev. Lett. 50 (25) (1983) 2024–2027.
- [11] G.B. Johnston, E.O. Hall, Studies on the heusler alloys—I. Cu2MnAl and associated structures, J. Phys. Chem. Solid 29 (2) (1968) 193–200.
- [12] A.M. Bratkovsky, Tunneling of electrons in conventional and half-metallic systems: towards very large magnetoresistance, Phys. Rev. B 56 (5) (1997) 2344–2347.
- [13] Z. Gercsi, et al., Spin polarization of Co2FeSi full-heusler alloy and tunneling magnetoresistance of its magnetic tunneling junctions, Appl. Phys. Lett. 89 (8) (2006).
- [14] S. Yamada, et al., Low-temperature grown quaternary heusler-compound Co2Mn1-xFexSi films on Ge(111), J. Appl. Phys. 109 (7) (2011).
- [15] T. Kimura, et al., Erratum: room-temperature generation of giant pure spin currents using epitaxial Co2FeSi spin injectors, NPG Asia Mater. 4 (3) (2012) e13–e.
- [16] L. Ritchie, et al., Magnetic, structural, and transport properties of the heusler alloysCo2MnSiand NiMnSb, Phys. Rev. B 68 (10) (2003).
- [17] A. Pfeiffer, et al., Spin currents injected electrically and thermally from highly spin polarized Co2MnSi, Appl. Phys. Lett. 107 (8) (2015).
- [18] W.H. Wang, et al., Magnetic properties and spin polarization of Co2MnSiHeusler alloy thin films epitaxially grown on GaAs(001), Phys. Rev. B 71 (14) (2005).
- [19] S. Aron-Dine, et al., First-principles investigation of structural and magnetic disorder in CuNiMnAl and CuNiMnSn heusler alloys, Phys. Rev. B 95 (2) (2017).
- [20] Y. Feng, et al., The effect of disorder on electronic and magnetic properties of quaternary heusler alloy CoFeMnSi with LiMgPbSb-type structure, J. Magn. Magn. Mater. 378 (2015) 7–15.
- [21] Y. Han, et al., 171 scandium-based full heusler compounds: a comprehensive study of competition between XA and L21 atomic ordering, Results Phys. 12 (2019) 435–446.
- [22] X. Wang, et al., L21 and XA ordering competition in titanium-based full-heusler alloys, J. Mater. Chem. C 5 (44) (2017) 11559–11564.
- [23] X. Du, et al., Site preference, magnetic and electronic properties of half-metallic vanadium-based full heusler alloys, J. Magn. Magn. Mater. 517 (2021).
- [24] M. Meinert, et al., GW study of the half-metallic heusler compounds Co2MnSi and Co2FeSi, Phys. Rev. B 86 (24) (2012).
- [25] J.P. Perdew, K. Burke, M. Ernzerhof, Generalized gradient approximation made simple, Phys. Rev. Lett. 77 (18) (1996) 3865–3868.
- [26] A. Dal Corso, Pseudopotentials periodic table: from H to pu, Comput. Mater. Sci 95 (2014) 337–350.
- [27] M. Meinert, Modified becke-Johnson potential investigation of half-metallic heusler compounds, Phys. Rev. B 87 (4) (2013).
- [28] F. Meng, et al., Site preference of zr in heusler alloys Zr2YAl (Y = cr, mn, fe co, ni) and its influence on the electronic properties, J. Alloy. Compd. 695 (2017) 2005 2001
- [29] H. Luo, et al., Competition of L21 and XA structural ordering in heusler alloys X2CuAl (X = sc, ti, V, cr, mn, fe co, ni), J. Alloy. Compd. 665 (2016) 180–185.
- [30] L. Wollmann, et al., Magnetism in cubic manganese-rich heusler compounds, Phys. Rev. B 90 (21) (2014).
- [31] A. Williams, et al., Generalized slater-pauling curve for transition-metal magnets, IEEE Trans. Magn. 19 (5) (1983) 1983–1988.
- [32] J.C. Slater, The ferromagnetism of nickel, II. Temperature Effects. Physical Review 49 (12) (1936) 931–937.
- [33] L. Pauling, The nature of the interatomic forces in metals, Phys. Rev. 54 (11) (1938) 899–904.
- [34] S. Skaftouros, et al., Generalized slater-pauling rule for the inverse heusler compounds, Phys. Rev. B 87 (2) (2013).
- [35] H.C. Kandpal, G.H. Fecher, C. Felser, Calculated electronic and magnetic properties of the half-metallic, transition metal based heusler compounds, J. Phys. D Appl. Phys. 40 (6) (2007) 1507–1523.